Nonlinear Reconstruction

Hong-Ming Zhu,[1,2] Yu Yu,[3] Ue-Li Pen,[4,5,6,7] Xuelei Chen,[1,2,8] and Hao-Ran Yu[9,4]

[1]*Key Laboratory for Computational Astrophysics, National Astronomical Observatories, Chinese Academy of Sciences, 20A Datun Road, Beijing 100012, China*
[2]*University of Chinese Academy of Sciences, Beijing 100049, China*
[3]*Key Laboratory for Research in Galaxies and Cosmology, Shanghai Astronomical Observatory, Chinese Academy of Sciences, 80 Nandan Road, Shanghai 200030, China*
[4]*Canadian Institute for Theoretical Astrophysics, University of Toronto, 60 St. George Street, Toronto, Ontario M5S 3H8, Canada*
[5]*Dunlap Institute for Astronomy and Astrophysics, University of Toronto, 50 St. George Street, Toronto, Ontario M5S 3H4, Canada*
[6]*Canadian Institute for Advanced Research, CIFAR Program in Gravitation and Cosmology, Toronto, Ontario M5G 1Z8, Canada*
[7]*Perimeter Institute for Theoretical Physics, 31 Caroline Street North, Waterloo, Ontario, N2L 2Y5, Canada*
[8]*Center of High Energy Physics, Peking University, Beijing 100871, China*
[9]*Kavli Institute for Astronomy and Astrophysics, Peking University, Beijing 100871, China*

(Dated: November 26, 2016)

We present a direct approach to non-parametrically reconstruct the linear density field from an observed non-linear map. We solve for the unique displacement potential consistent with the non-linear density and positive definite coordinate transformation using a multigrid algorithm. We show that we recover the linear initial conditions up to $k \sim 1$ h/Mpc with minimal computational cost.

This reconstruction approach generalizes the linear displacement theory to fully non-linear fields, potentially substantially expanding the BAO and RSD information content of dense large scale structure surveys, including for example SDSS main sample and 21cm intensity mapping.

PACS numbers:

Introduction.—The observation of cosmological large scale structure is a cornerstone of modern cosmology. Ambitious surveys are mapping large swaths of the visible universe (e.g. CHIME [1], Tianlai [2], DESI [3], PFS [4], etc). Precision measurements of baryon acoustic oscillations, redshift space distortions, and primordial non-Gaussianity, etc are continually improving. However, the precision of the measurement is often limited by strong non-Gaussianity of the dark matter and galaxy density fields on small scales, which prevent a simple mapping to the initial conditions that are predicted by cosmological theories. The loss of coherence to the initial conditions has been known as mode-mode coupling, information saturation, etc.

Some of the couplings are understood as arising from the coupling of large scale linear modes to smaller scale still linear modes (e.g. cosmic tides [5–7], super-sample covariance [8–10]). These can be corrected by a linear mapping, also known as "reconstruction" [11].

Recent work has showed that the Lagrangian nonlinear displacement potential at $z = 0$ correlates with the initial linear field to $k \sim 2$ h/Mpc, about an order of magnitude shorter length scale than observed in Eulerian space [12]. That requires knowing the actual displacement of dark matter particles, which in practice is not observable. In this paper we implement the combination of the mass ordering coordinate of [13] with the E-mode displacement field, resulting in a unique solution that has a comparable reconstruction fidelity as the true E-mode displacement field.

The E-mode displacement.—In the Lagrangian picture of structure formation, the displacement field $\boldsymbol{s}(\boldsymbol{q}, t)$ fully describes the motion of each mass element. The Eulerian position $\boldsymbol{x}(\boldsymbol{q}, t)$ of a mass element is given by

$$\boldsymbol{x}(\boldsymbol{q}, t) = \boldsymbol{q} + \boldsymbol{s}(\boldsymbol{q}, t), \tag{1}$$

where $\boldsymbol{q}$ is the initial Lagrangian position of this mass element. The displacement field $\boldsymbol{s}(\boldsymbol{q})$ can be decomposed into a gradient part and a curl part,

$$\boldsymbol{s}(\boldsymbol{q}) = \boldsymbol{s}_E(\boldsymbol{q}) + \boldsymbol{s}_B(\boldsymbol{q}), \tag{2}$$

where $\nabla \times \boldsymbol{s}_E = 0$ and $\nabla \cdot \boldsymbol{s}_B = 0$. The E-mode displacement can be completely described by a scalar potential, while the B-mode displacement has two independent components. Since from cosmological observations we only have the density field, which is a scalar field, we expect to reconstruct the E-mode displacement field.

Reconstruction algorithm.—The observed matter distribution is rather inhomogeneous due to nonlinear gravitational clustering. However, the density field is homogeneous in the mass coordinate as the initial matter distribution. The basic idea of reconstrution is to build a curvilinear coordinate system $\boldsymbol{\xi} \equiv (\xi_1, \xi_2, \xi_3)$, where the mass per volume element is constant. In order to determine the physical position of each lattice point, we need to specify the Cartesian coordinate $\boldsymbol{x}(\boldsymbol{\xi}, t)$ of each curvilinear coordinate. Since we attempt to follow the potential flow instead of the vorticity, we define a coor-

dinate transformation that is a pure gradient,

$$x^i = \xi^\mu \delta^i_\mu + \Delta x^i, \tag{3}$$

where

$$\Delta x^i \equiv \frac{\partial \phi}{\partial \xi^\nu} \delta^{i\nu}. \tag{4}$$

Here, ϕ is called the *displacement potential*. The new coordinate frame gives the estimated initial Lagrangian coordinates. The difference between these two frames is the estimated nonlinear displacement field. Here, Latin indices denote Cartesian coordinate labels x^i, while Greek indices denote the curvilinear coordinates ξ^α.

The problem simplifies to find the displacement potential, where the density field is constant in the curvilinear coordinate system. One efficient and robust algorithm is the moving mesh approach, which is originally introduced for the adaptive particle-mesh N-body algorithm [14] and the moving mesh hydrodynamics algorithm [15]. The moving grid based simulation algorithm adopts a curvilinear moving grid, which evolves towards a state of constant mass per grid cell, to maintain constant resolution in mass. The evolution of the curvilinear moving grid is determined by a linear elliptic evolution equation

$$\partial_\mu (\rho \sqrt{g} e^\mu_i \delta^{i\nu} \partial_\nu \dot{\phi}) = \Delta \rho, \tag{5}$$

where e^μ_i is the matrix inverse of the triad $e^i_\mu = \partial x^i / \partial \xi^\mu$, $\sqrt{g} = \det(\partial x^i / \partial \xi^\alpha)$ and $\Delta\rho = \bar{\rho} - \rho\sqrt{g}$. See Ref. [14] for a simple physical interpretation of Eq. (5). The ellipitic equation can be solved using the multigrid algorithm described in Ref. [14].

Since the displacement from the initial Lagrangian position to the final Eulerian position can be large, the elliptic equation must then be solved perturbatively. We obtain the change of the displacement potential $\Delta\phi = \dot{\phi}\Delta t$ at each time step and then update the density field in the new coordinate frame. The solution is given by

$$\phi = \Delta\phi^{(1)} + \Delta\phi^{(2)} + \Delta\phi^{(3)} + \cdots \tag{6}$$

where $\Delta\phi^{(i)}$ is the result from the ith iteration. We also implement the smoothing and limiting schemes to guarantee the triad e^μ_i is positive definite [14, 15], from which we have the relation $\partial x^a / \partial \xi^a > 0$ (no summation). From this equality, it follows that each Cartesian coordinate increases monotonically as a function of its corresponding curvilinear coordinate. The displacement potential consistent with the positive definite coordinate transformation is unique. Then, the divergence of the estimated displacement gives the reconstructed density field

$$\delta_r(\boldsymbol{\xi}) = -\nabla \cdot \Delta \boldsymbol{x}(\boldsymbol{\xi}) = -\nabla^2 \phi(\boldsymbol{\xi}), \tag{7}$$

where $\boldsymbol{\xi}$ is the estimated initial Lagrangian coordinate. In the case that particles follow a irrotational potential flow and no shell crossing happens, the reconstructed displacement is exact up to a global spatial translation. However, shell crossing happens in the nonlinear regime. This reconstruction algorithm gives an approximate solution.

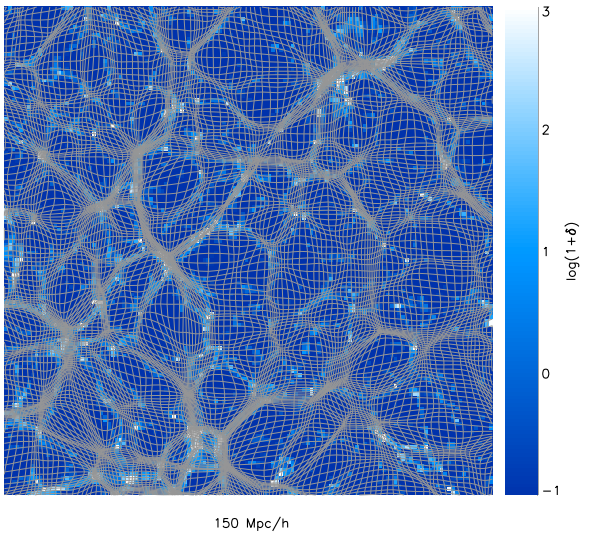

FIG. 1: The nonlinear density field at $z = 0$ and the projected deformed grid from reconstruction. The grid lines show strong correlation with the filamentary structures.

Implementation and results.—To test the performance of the new reconstruction algorithm, we run N-body simulations with the CUBEP^{3}M code [16]. The simulation involves 2048^3 dark matter particles in a box of side length 600 Mpc/h. In the analysis, we use the output at $z = 0$. Mass densities are computed on 512^3 grids. The nonlinear reconstruction code is based on the `CALDEFP` subroutine from the moving mesh hydrodynamics code [15]. The nonlinear reconstruction code solves the displacement potential iteratively. We test convergence by comparing results from different time steps and find the reconstruction converges after 1500 time steps for the nonlinear density field on 512^3 grids. We also scale the initial density field at $z = 100$ by the linear growth factor to get the linear density field at $z = 0$.

Figure 1 shows a slice of the nonlinear density field. We also plot the deformed grid on the density field. The grid becomes denser in the higher density region and sparser in the lower density region. The grid lines also show strong correlation with the filamentary structures. The difference between the regular grid and the deformed grid is the estimated displacement field and its divergence gives the reconstructed linear density field. The nonlinear density field $\delta(\boldsymbol{x})$ is given on the Eulerian position $\boldsymbol{x}$, while the reconstructed density field $\delta_r(\boldsymbol{\xi})$ is computed on the estimated Lagrangian position $\boldsymbol{\xi}$. Due to the limiting and smoothing schemes we use, the grid never overlaps

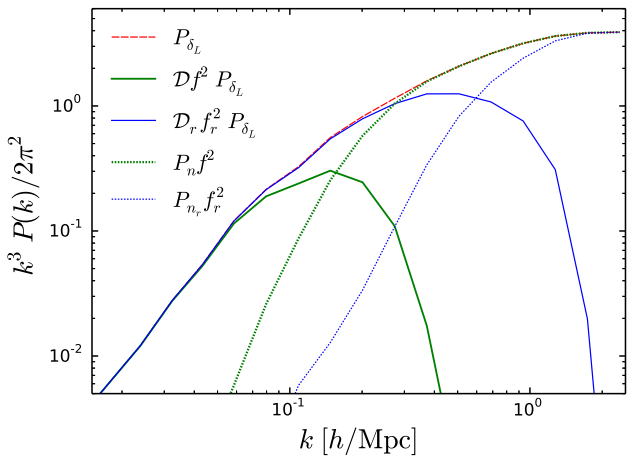

FIG. 2: The linear power spectrum (dashed line), the linear parts of the nonlinear (thick solid line) and reconstructed (thin solid line) power spectra, the noise parts of the nonlinear (thick dotted line) and reconstructed (thin dotted line) power spectra. For visual comparisions, we rescale both the linear and noise parts by $f^2 = P_{\delta_L}/P_\delta$ and $f_r^2 = P_{\delta_L}/P_{\delta_r}$ for the nonlinear and reconstructed fields, respectively. The noise terms dominate over the signals at $k \gtrsim 0.1\ h/\mathrm{Mpc}$ for the nonlinear field and $k \gtrsim 0.6\ h/\mathrm{Mpc}$ for the reconstructed field.

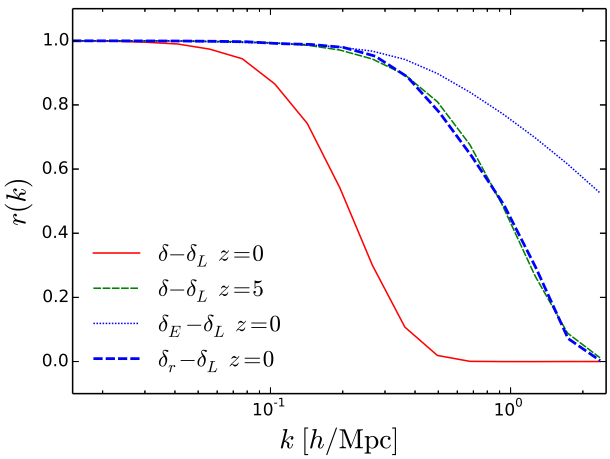

FIG. 3: The $\delta - \delta_L$ correlation coefficients at $z = 0$ (solid line) and $z = 5$ (thin-dashed line), the $\delta_E - \delta_L$ correlation coefficient (dotted line), as well as the $\delta_r - \delta_L$ correlation coefficient (thick-dashed line).

itself as in Refs. [14, 15].

To directly quantify the linear information in the reconstructed density field, we decompose the reconstructed density field δ_r as

$$\delta_r(k) = b_r(k)\delta_L(k) + n_r(k), \tag{8}$$

where $b_r(k) = P_{\delta_r\delta_L}(k)/P_{\delta_L}(k)$. Here, $b_r\delta_L$ is completely correlated with the linear density field δ_L and n_r uncorrelated with the linear density field δ_L. The power spectrum of the reconstructed field can be written as

$$P_{\delta_r}(k) = \mathcal{D}_r(k)P_{\delta_L}(k) + P_{n_r}(k), \tag{9}$$

where $\mathcal{D}_r = b_r^2$ is the nonlinear damping factor. For the nonlinear density field, we also have

$$P_\delta(k) = \mathcal{D}(k)P_{\delta_L}(k) + P_n(k), \tag{10}$$

where $\mathcal{D} = b^2$ and $b = P_{\delta\delta_L}/P_{\delta_L}$. In Fig. 2, we plot the linear components and the noise terms of the nonlinear and reconstructed power spectra. The noise part dominates over the linear signal at $k \gtrsim 0.6\ \mathrm{Mpc}/h$, indicating that all BAO peaks can be measured to unprecedented accuracy.

Reconstruction reduces the nonlinear damping $\mathcal{D}(k)$ as well as the noise term $P_n(k)$. To quantify the overall performance, we can use the cross-correlation coefficient

$$r(k) = \frac{P_{\delta\delta_L}(k)}{\sqrt{P_\delta(k)P_{\delta_L}(k)}} = \frac{1}{\sqrt{1+\eta(k)}}, \tag{11}$$

where $\eta = P_n/(b^2P_{\delta_L})$ quantifies the relative amplitude of n with respect to $b\delta_L$. In Fig. 3, we plot the cross-correlation coefficients. The correlation of the reconstructed field δ_r with the linear density field δ_L is almost the same as that of the nonlinear density field δ at $z = 5$, which is better than the 1D case, where the correlation of δ_r with δ_L is only comparable to that of δ at $z = 3$ [13]. This is also as expected since the nonlinear evolution in 1D is more significant than the 3D case [17]. We also show the cross-correlation coefficient of δ_E with δ_L, where $\delta_E(\boldsymbol{q}) = -\nabla\cdot\boldsymbol{s}_E(\boldsymbol{q})$ is the negative divergence of the real E-mode displacement from simulation. It is still hard to recover linear modes at $k \gtrsim 1h/\mathrm{Mpc}$, since some information has been irreversibly lost in nonlinear evolution.

The density fluctuation probability distribution function (PDF) quantifies the Gaussianity of the density field. Figure 4 shows the PDFs of the density fields. Since the PDFs depend on the grid scale, we apply the Wiener filter

$$W(k) = \frac{P_{\delta_L}(k)}{P_{\delta_L}(k) + P_{n_r}(k)/b_r^2(k)} \tag{12}$$

to both the reconstructed and linear fields to get the converged results. The reconstructed density field is well correlated with the linear density field and also much more Gaussian than the original nonlinear density field. The new reconstruction method are expected to reduce the correlation between different k-bins and increase the information content [18–20]. Notice that the values of the reconstructed density δ_r are always smaller than 3. The compression limiter constrains $\partial x^a/\partial\xi^a \geq 0.1$ [14, 15]. The reconstructed density field is given by the negative divergence of the estimated nonlinear displacement field, $\delta_r = -\nabla\cdot\Delta\boldsymbol{x} = 3 - \nabla\cdot\boldsymbol{x}$, where $\nabla\cdot\boldsymbol{x} = \partial x^1/\partial\xi^1 +$

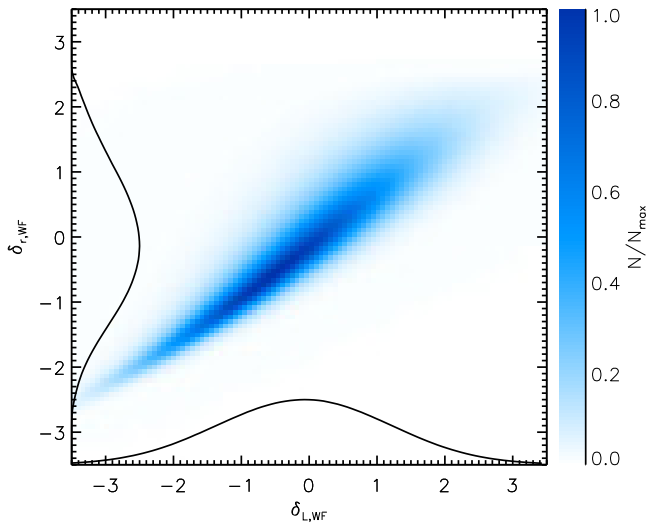

FIG. 4: The joint PDF of the reconstructed field δ_r and linear density field δ_L. We also plot the PDFs of δ_r and δ_L. Both fields have been Wiener filtered to get converged results. The value of the reconstructed density field is always smaller than 3.

$\partial x^2/\partial\xi^2 + \partial x^3/\partial\xi^3$. We find the maximum value is 2.7 for the reconstructed densities. This has confirmed that we have a continuous sequence of nondegenerate triads in the reconstruction. In the 1D case, the maximum value is 1 since we only have one spatial dimension in the 1D cosmology [13].

Discussions.—The Lagrangian BAO reconstruction algorithm involves displacing individual objects according to the linear displacement that is computed from the observed galaxy distribution under certain model assumptions (the fiducial cosmology, galaxy bias, growth rate, etc) [11, 21]. The results depend on the assumed fiducial model and must be tested against different parameter choices, which is computationally expensive [22]. The reconstruction of the displacement potential consistent with the nonlinear density and positive definite coordinate transformation is a purely mathematical problem with no cosmological dynamics involved. The implementation of the new reconstruction algorithm does not require any model assumptions. The new algorithm recovers the linear density modes to $k \sim 0.6$ h/Mpc, which include about all the BAO information. This has significant implications for the measurement of BAO in dense large scale structure surveys such as SDSS main sample and 21 cm intensity mapping. To apply the new reconstruction method to observations, we need to consider reconstruction from galaxies or halos with redshift space distortions. We intend to investigate these in subsequent works.

The observed position of a mass element will be shifted by its peculiar velocity along the line of sight, which corresponds to a simple additive offset of the displacement field. The displacement field solved from the observed density field automatically includes the additive offset. Since much less nonlinearities involved in the displacement potential, the modeling of RSD will be improved significantly.

Most of methods to reconstruct the velocity field from the observed density field are based on the linearized continuity equation. The observed nonlinear density field is usually smoothed on the linear scale ($\sim$ 10 Mpc/h) to make the linear approximation valid. We can also reconstruct the velocity field from the estimated displacement field. This requires a detailed study of the correlation between the displacement field and the velocity field, which will be presented in future.

Neutrinos are expected to suppress the growth of structure on scales below the neutrino thermal free-streaming scale [23]. It is interesting to study the effect of neutrinos on the Lagrangian space clustering, where the nonlinear evolution is less substantial. The reconstruction method is also crucial for measuring the dark matter-neutrino cross correlation dipole in Lagrangian space [24, 25].

The simulations are performed on the BGQ supercomputer at the SciNet HPC Consortium. SciNet is funded by the Canada Foundation for Innovation under the auspices of Compute Canada, the Government of Ontario, the Ontario Research Fund Research Excellence, and the University of Toronto. We acknowledge the support of the Chinese MoST 863 program under Grant No. 2012AA121701, the CAS Science Strategic Priority Research Program XDB09000000, the NSFC under Grant No. 11373030 and No. 11403071, IAS at Tsinghua University, and NSERC. The Dunlap Institute is funded through an endowment established by the David Dunlap family and the University of Toronto. Research at the Perimeter Institute is supported by the Government of Canada through Industry Canada and by the Province of Ontario through the Ministry of Research & Innovation.

[1] K. Bandura, G. E. Addison, M. Amiri, J. R. Bond, D. Campbell-Wilson, L. Connor, J.-F. Cliche, G. Davis, M. Deng, N. Denman, et al., in *Ground-based and Airborne Telescopes V* (2014), vol. 9145 of Proc. SPIE, p. 914522, 1406.2288.

[2] Y. Xu, X. Wang, and X. Chen, ApJ **798**, 40 (2015), 1410.7794.

[3] DESI Collaboration, A. Aghamousa, J. Aguilar, S. Ahlen, S. Alam, L. E. Allen, C. Allende Prieto, J. Annis, S. Bailey, C. Balland, et al., ArXiv e-prints (2016), 1611.00036.

[4] M. Takada, R. S. Ellis, M. Chiba, J. E. Greene, H. Aihara, N. Arimoto, K. Bundy, J. Cohen, O. Doré, G. Graves, et al., PASJ **66**, R1 (2014), 1206.0737.

[5] U.-L. Pen, R. Sheth, J. Harnois-Deraps, X. Chen, and Z. Li, ArXiv e-prints (2012), 1202.5804.

[6] H.-M. Zhu, U.-L. Pen, Y. Yu, X. Er, and X. Chen, Phys. Rev. D **93**, 103504 (2016), 1511.04680.
[7] K. Akitsu, M. Takada, and Y. Li, ArXiv e-prints (2016), 1611.04723.
[8] M. Takada and W. Hu, Phys. Rev. D **87**, 123504 (2013), 1302.6994.
[9] Y. Li, W. Hu, and M. Takada, Phys. Rev. D **89**, 083519 (2014), 1401.0385.
[10] Y. Li, W. Hu, and M. Takada, Phys. Rev. D **90**, 103530 (2014), 1408.1081.
[11] D. J. Eisenstein, H.-J. Seo, E. Sirko, and D. N. Spergel, ApJ **664**, 675 (2007), astro-ph/0604362.
[12] H.-R. Yu, U.-L. Pen, and H.-M. Zhu, ArXiv e-prints (2016), 1610.07112.
[13] H.-M. Zhu, U.-L. Pen, and X. Chen, ArXiv e-prints (2016), 1609.07041.
[14] U.-L. Pen, ApJS **100**, 269 (1995).
[15] U.-L. Pen, ApJS **115**, 19 (1998), astro-ph/9704258.
[16] J. Harnois-Déraps, U.-L. Pen, I. T. Iliev, H. Merz, J. D. Emberson, and V. Desjacques, MNRAS **436**, 540 (2013), 1208.5098.
[17] M. McQuinn and M. White, J. Cosmology Astropart. Phys. **1**, 043 (2016), 1502.07389.
[18] A. Meiksin and M. White, MNRAS **308**, 1179 (1999), astro-ph/9812129.
[19] R. Scoccimarro, M. Zaldarriaga, and L. Hui, ApJ **527**, 1 (1999), astro-ph/9901099.
[20] C. D. Rimes and A. J. S. Hamilton, MNRAS **360**, L82 (2005), astro-ph/0502081.
[21] M. Schmittfull, Y. Feng, F. Beutler, B. Sherwin, and M. Y. Chu, Phys. Rev. D **92**, 123522 (2015), 1508.06972.
[22] N. Padmanabhan, X. Xu, D. J. Eisenstein, R. Scalzo, A. J. Cuesta, K. T. Mehta, and E. Kazin, MNRAS **427**, 2132 (2012), 1202.0090.
[23] J. R. Bond, G. Efstathiou, and J. Silk, Physical Review Letters **45**, 1980 (1980).
[24] H.-M. Zhu, U.-L. Pen, X. Chen, D. Inman, and Y. Yu, Physical Review Letters **113**, 131301 (2014), 1311.3422.
[25] H.-M. Zhu, U.-L. Pen, X. Chen, and D. Inman, Physical Review Letters **116**, 141301 (2016).